Clim. Past, 20, 1703–1720, 2024
https://doi.org/10.5194/cp-20-1703-2024

Climate of the Past
Open Access
EGU

Patterns of centennial to millennial Holocene climate variation in the North American mid-latitudes

Bryan N. Shuman

Department of Geology and Geophysics, University of Wyoming, Laramie, WY 82071, USA

Correspondence: Bryan N. Shuman (bshuman@uwyo.edu)

Received: 14 November 2022 – Discussion started: 28 November 2022
Revised: 13 February 2024 – Accepted: 17 February 2024 – Published: 1 August 2024

Abstract. Noise in Holocene paleoclimate reconstructions can hamper the detection of centennial to millennial climate variations and diagnoses of the dynamics involved. This paper uses multiple ensembles of reconstructions to separate signal and noise and determine what, if any, centennial to millennial variations influenced North America during the past 7000 years. To do so, ensembles of temperature and moisture reconstructions were compared across four different spatial scales: multi-continent, regional, sub-regional, and local. At each scale, two independent multi-record ensembles were compared to detect any centennial to millennial departures from the long Holocene trends, which correlate more than expected from random patterns. In all cases, the potential centennial to millennial variations had small magnitudes. However, at least two patterns of centennial to millennial variability appear evident. First, large-scale variations included a prominent Mid-Holocene anomaly from 5600–5000 yr BP that increased mean effective moisture and produced temperature anomalies of different signs in different regions. The changes shifted the north–south temperature gradient in mid-latitude North America with a pattern similar to that of the North Atlantic Oscillation (NAO). Second, correlated multi-century (∼ 350 years) variations produce a distinct spectral signature in temperature and hydroclimate records along the western Atlantic margin. Both patterns differ from random variations, but they express distinct spatiotemporal characteristics consistent with separate controlling dynamics.

1 Introduction

A prominent gap in the conceptual and empirical understanding of the full spectrum of climate variation exists at centennial to millennial (cen–mil) scales, particularly for warm climate states (Crucifix et al., 2017; Hernández et al., 2020; Wanner et al., 2008). Cen–mil variations exceed the scales of direct observation and yet are short relative to the resolution of many geological records. Climate models can also fail to sufficiently resolve this scale of climate variation, which is particularly important for anticipating regional changes (Hébert et al., 2022; Laepple et al., 2023). The resulting gap in understanding has been recognized for decades (Saltzman, 1982) and continues to thwart efforts to understand "low-frequency" components of change during the Common Era and other times (Ault et al., 2013). The Holocene Epoch offers a key to this "missing" scale because cen–mil variability across a broad continuum (Hernández et al., 2020; Huybers and Curry, 2006; Mayewski et al., 2004; Wanner et al., 2008; Hébert et al., 2022) likely played an important role in shaping ecological, geomorphic, and human history during the past 11 700 years (Fletcher et al., 2013; Shuman et al., 2019; deMenocal, 2001).

Cen–mil variation during the Holocene must have arisen from the interaction among (1) deterministic changes, such as energy balance responses to seasonal insolation trends; (2) chaotic dynamics, such as the fluid behaviors of the atmosphere and oceans and complex biosphere feedbacks; and (3) stochastic events and variability, such as is common on interannual to decadal scales. Non-linear, probabilistic, or transient cen–mil dynamics may have followed the Holocene's orbital and greenhouse gas changes (Claussen et al., 1999; Saltzman, 1982; Wan et al., 2019), autoregressive solar variations (Renssen et al., 2006), and stochastic volcanic eruptions

(Kobashi et al., 2017). However, intrinsic, unforced cen–mil variability arising from atmospheric, ocean, and sea ice dynamics may have been equally as significant (Ault et al., 2018), with ocean variability driving regional change even over the continents (Hébert et al., 2022). Simulations produce repeated unforced millennial variations, which are similar in magnitude to the effects of early Holocene meltwater forcing and are correlated over the northern continents and oceans (Marsicek et al., 2018; Wan et al., 2019). Some variations likely centered on the North Atlantic (Thornalley et al., 2009; Anchukaitis et al., 2019) and the tropical Pacific (Karnauskas et al., 2012) with the potential for far-reaching spatial expressions like those expressed at other timescales. Biosphere feedbacks may have also triggered state shifts against the backdrop of other Holocene variability (Claussen et al., 1999; deMenocal et al., 2000). Importantly, internal variability may generate variations in the opposing sign in different regions with areas of change and no change in close proximity (Shuman et al., 2023).

A daunting breadth of variation among individual records matches the wide range of possible drivers (Mayewski et al., 2004; Wanner et al., 2008), but signal-to-noise ratios are small. Analytical or calibration uncertainties of ~ 2°C (e.g., Russell et al., 2018; Williams and Shuman, 2008; Martínez-Sosa et al., 2021) often dwarf the expected magnitudes of cen–mil temperature variation during the Holocene (~ 0.5 °C in CCSM3 TRACE simulations; Marsicek et al., 2018; Wan et al., 2019). At the same time, reconstruction techniques, age uncertainties, and averaging across multiple records can reduce the apparent amplitude of cen–mil climate variations (Hébert et al., 2022). Furthermore, slow Earth system components like the ocean can integrate stochastic interannual variability to produce autoregressive variations at cen–mil scales (Huybers and Curry, 2006), but oscillations in many paleoclimate datasets may be noise-generated by smoothing or other integrating processes. Statistical transformations (e.g., curve fitting); sampling effects (e.g., homogenized samples spanning decades); and a wide range of environmental filtering processes such as sediment mixing, lake residence times, or slow forest turnover add temporal autocorrelation generating oscillations from white noise via the Slutzky–Yule effect (Slutzky, 1937). Diagnosing the continuum of weak signals and their complex interactions amid the full array of noise and uncertainties creates a unique challenge for studying cen–mil variability but is essential for determining the origins of changes that may modify future trends, particularly at regional and finer spatial scales.

The goal of developing a "coherent, falsifiable narrative" (Bender, 2013) may help: what signals are coherent among independent datasets? Are they falsifiably different from null expectations about noise? This paper applies these questions to cen–mil variations during the past 7000 years, after ice sheet influences diminished. The analyses focus on variations previously observed at four spatial scales centered on eastern mid-latitude North America to describe the types of Holocene variations expressed in the northern mid-latitudes. Cen–mil variations in this region include long-term dynamics similar to the interannual North Atlantic Oscillation (NAO; Olsen et al., 2012; Orme et al., 2021; Shuman et al., 2023), correlations among North American droughts and Atlantic temperatures (Shuman et al., 2019; Shuman and Burrell, 2017; Anchukaitis et al., 2019), and possible large-scale temperature variations consistent in frequency and magnitude with unforced variability simulated by models (Marsicek et al., 2018; Herzschuh et al., 2023). To compare the expression of cen–mil variability across spatial scales, dissimilar geographic regions, and different climate variables, the analyses used here focus on a spatial hierarchy of paired multi-record ensembles. The scales span from hemispheric variations that extend well beyond North America to sub-regional and local variations that differ among areas of the continent, as follows:

- multi-continent cen–mil signals in both a temperature ensemble derived from European and North American pollen records and an ensemble of water temperature records (Marsicek et al., 2018) (Fig. 1a);
- regional cen–mil signals in networks of temperature and moisture records spanning mid-latitude North America (Shuman and Marsicek, 2016) (Fig. 1b);
- sub-regional cen–mil signals in reconstructions from the central and northeastern sub-regions of mid-latitude North America (Shuman and Burrell, 2017; Shuman and Marsicek, 2016) (Fig. 1b); and
- site level cen–mil signals within the sub-regions, including individual temperature and hydroclimate records (Shuman and Burrell, 2017; Shuman and Marsicek, 2016) (individually labeled sites; Fig. 1b).

The analyses build upon the detection of cen–mil signals that were cross-validated across sites and multiple lines of evidence in the northeastern US (Shuman et al., 2019) and compares them to evidence of different cen–mil signals at the larger regional (Shuman and Marsicek, 2016) and continental scales (Marsicek et al., 2018). To help evaluate potential cen–mil variations, correlations among paleoclimate reconstructions were evaluated at different frequencies and compared against the level of spurious correlations in random data series (Reschke et al., 2019). Random series reveal signal characteristics, such as the strength of signal magnitudes and correlations among multi-record ensemble means, which could help distinguish between cen–mil noise and climatically significant variations (Fig. 2). To further diagnose the variations, spatial patterns associated with temperature change at 5500–5000 yr BP are also evaluated; the interval represents the largest rate of change in pollen-inferred temperatures, lake level changes, and stable isotope records from mid-latitude North America (Shuman and Marsicek, 2016) and includes a potential step shift in hemispheric temperatures (Marsicek

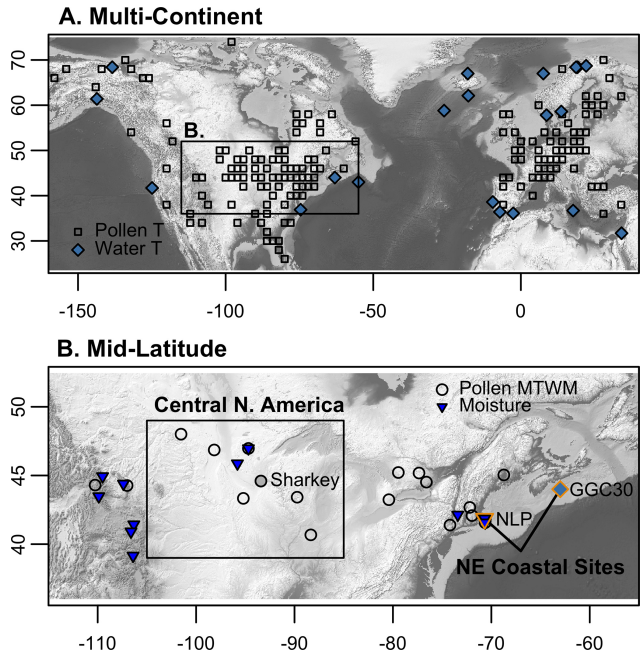

Figure 1. Locations of paleoclimate reconstructions incorporated into ensembles of **(a)** continental-scale mean annual temperatures (pollen T, squares; Marsicek et al., 2018) and water temperatures (water T, blue circles; from Marcott et al., 2013). **(b)** Mid-latitude, central, and northeastern (NE) coastal mean temperatures of the warmest month (MTWM, circles; Shuman and Marsicek, 2016) and moisture availability (blue triangles; Shuman and Marsicek, 2016). The mid-latitude ensembles include all pollen-inferred MTWM and moisture records shown in panel **(b)**. The central North America ensembles include only sites in the inset box, and the NE coastal comparison uses the two sites outlined in orange (New Long Pond, NLP; Newby et al., 2014; OCE326-GGC30, a water temperature site in panel **(a)** from Sachs, 2007). In the central region, the MTWM mean excludes and is compared to Sharkey Lake, MN (gray). ETOPO2022 forms the base map (NOAA NCEI, 2022).

et al., 2018). The Mid-Holocene changes may relate to commonly detected anomalies in many North American records and could have characteristics (i.e., changes in the latitudinal temperature gradient over North America) similar to the NAO at interannual scales (Hurrell et al., 2003; Folland et al., 2009; Shuman et al., 2023). Together, the results demonstrate a set of cen–mil changes over the past 7000 years, which correlate among ensembles of temperature and moisture reconstructions while differing among regions and scales (likely because they represent multiple dynamics).

2 Methods

For this analysis, cen–mil variations in Holocene paleoclimate time series are defined as variations evident in paleoclimate reconstructions that have been binned at 100-year time steps and then detrended using a Gaussian filter with a 6000-year window (see Reschke et al., 2019). They are considered significant and therefore climatically meaningful if they are correlated in independent paleoclimate reconstructions more than expected from surrogate time series randomly generated as power law time series with the same spectral slope over the 100–2000-year band of variation as determined from the paleoclimate reconstructions (following Reschke et al., 2019).

All of the paleoclimate datasets examined here have been previously published. Additional data may help further evaluate the patterns involved, but this paper aims to interrogate and compare the patterns over the past 7000 years in these specific representative datasets to generate an initial evaluation of possible patterns.

At the largest (multi-continent) scale (Fig. 1a), Marsicek et al. (2018) used 642 fossil pollen records, which were averaged over a grid, to reconstruct Holocene mean annual temperature (MAT) trends across Europe and North America (grid points used for the reconstruction are shown as squares in Fig. 1a). They showed cen–mil variations which correlated across the two continents, between random subsets of the reconstructions, and with those detected in an ensemble of geochemical and chironomid-inferred water temperature records from marine and lake cores in the North American–European region (blue circles, Fig. 1a). The mean European and North American MAT reconstruction and the water temperature ensemble are used here as two independent records of possible large-scale cen–mil variations, which may have had consequences in mid-latitude North America.

At the mid-latitude (regional) scale (Fig. 1b), Shuman and Marsicek (2016) synthesized 40 well-resolved paleoclimate records from across mid-latitude North America. They produced independent reconstructions of (1) the regional mean temperature of the warmest month (MTWM), averaged from 16 pollen-inferred records (circles, Fig. 1b), and (2) effective moisture, reconstructed using 9 lake level and 2 dust records averaged as z scores (blue triangles; Fig. 1b). The cen–mil variations in the independent MTWM and moisture reconstructions have not been previously compared. To evaluate the spatial patterns involved in the most prominent variation, an unusually cool period from 5600–5000 yr BP, the MTWM dataset is also split here into two subsets for comparison based on the direction of the previously identified Mid-Holocene temperature change (Shuman and Marsicek, 2016; Shuman et al., 2023). Sites were selected by dividing the records into two groups based on the mean difference in MTWM between two 600-year periods (5600–5000 – 4700–4100 yr BP) (Fig. 3c; Shuman and Marsicek, 2016). The mean change across the 600-year periods was used to minimize any artificial alignment of noise in the data caused by randomly splitting the data based on changes at a narrow, fixed point in time. Ensemble means with uncertainty distributions for each group were produced by randomly selecting and averaging five individual pollen-inferred MTWM records, which were selected from each group with replacement 100 times. A comparison is also made with geochemical data from the two areas.

At finer scales, Shuman and Marsicek (2016) also produced sub-regional temperature and moisture reconstructions based on the averages of records from geographically distinct areas, including in central North America and the northeastern coast (Fig. 1b). The resulting MTWM and moisture reconstructions from central North America are used here to examine cen–mil variation in a mid-continent sub-region (inset box, Fig. 1b). The central sub-region ensemble incorporates six pollen-inferred MTWM reconstructions from North Dakota, Minnesota, Iowa, Wisconsin, and Illinois; moisture history was reconstructed from two dust records from Minnesota. One centrally located MTWM reconstruction based on fossil pollen data from Sharkey Lake, Minnesota (Camill et al., 2003), is excluded and compared with the sub-regional ensemble to confirm the sub-regional pattern and represent the local-scale expression of the cen–mil variations (gray circle, Fig. 1b).

For comparison, and to further evaluate cen–mil variation at the finest local scale, two individual records from the northeastern (NE) coast of North America are used (orange outlined symbols, Fig. 1b). The records are representative of the NE coastal sub-region and have been identified as having correlated cen–mil temperature and moisture variations (Shuman et al., 2019; Shuman and Burrell, 2017; Shuman and Marsicek, 2016). The alkenone-inferred sea surface temperature (SST) reconstruction from the Scotian Margin, core OCE326-GGC30 (Sachs, 2007), is used to capture sub-regional temperature variations; its temperature variations correlate with those represented by the regional MTWM reconstruction in Shuman and Marsicek (2016) and based on five fossil pollen sites from the northeastern US. The lake level reconstruction from New Long Pond, Massachusetts, is highly correlated with similar reconstructions from other nearby lakes (Newby et al., 2014; Shuman and Burrell, 2017) and with pollen-inferred precipitation changes at five fossil pollen sites from same area (Shuman et al., 2019). Synchrony analyses of the calibrated radiocarbon dates used to constrain the paleo-shoreline deposits support the cen–mil details of the lake level reconstruction by confirming synchronous changes in multiple lakes (Newby et al., 2014), and the pollen-inferred precipitation reconstructions accurately inform simulations of the stratigraphic record of lake level changes using forward-modeling approaches (Shuman et al., 2019). For this reason, the analysis here focuses on temperature–moisture correlations between individual sites (including local noise but avoiding any effects of multi-site averaging) but is representative of sub-regional means from the coastal NE.

2.1 Analyses

To extract the cen–mil component of the eight datasets, curves were fit to the long-term trends using a Gaussian filter with a 6000-year window using the smoother package in R (R Core Development Team, 2020); analyses of the cen–mil variations then use the detrended time series derived from the residuals of the Gaussian smoother. The previously published confidence intervals from each of the eight datasets (Marsicek et al., 2018; Shuman and Marsicek, 2016; Shuman and Burrell, 2017) were also detrended by subtracting the same Gaussian filtered trends. Because most of the reconstructions represent multi-record ensembles, they have been previously interpolated and binned at 100- or 50-year time steps to combine the unevenly spaced individual data. Here, the 100-year time steps are used, given a mean sample resolution of 120 years per sample for the mid-latitude pollen records (Shuman and Marsicek, 2016). The resulting time series are smoothed and then detrended to focus on multi-century and longer patterns of variation.

Once detrended, Pearson's product moment correlation coefficients were calculated for comparison with null distributions. To do so, the CorQuantilesNullHyp function in the corit package in R was used to calculate Pearson's product moment correlation coefficients at specific timescales of variation, with periods ranging from 100–2000 years for comparison with null distributions of correlations among 1000 random surrogate power law time series with the same spectral slopes as the detrended reconstructions (Reschke et al., 2019). The independent data series for each scale or region were also compared using generalized least squares regression (gls in the mgvc package in R) to account for correlated errors by assuming a first-order moving average structure in the residuals; slopes of the regression line that differ significantly from zero provide additional evidence of a significant correlation. Spectral analyses were performed on the detrended cen–mil residuals using the multitaper package in R to compute multitaper spectral estimates (Percival et al., 1993). All of the analyses were applied only to 7000 years of data, although longer segments of the time series are also plotted.

2.2 Demonstration of random effects

The low signal-to-noise ratios and the timescale of cen–mil variation create particular challenges for detecting robust signals. Null expectations can help assess whether analyses show significant patterns (Reschke et al., 2019). To visually demonstrate the problem, 1000 random number series representing 11 000 simulated years were generated. For each series, 11 000 numbers were drawn from a normal distribution to produce time series of white noise. Loess curves with a 500-year span were then fit to each series to generate Slutzky–Yule oscillations by smoothing the random time series to produce cen–mil variations similar to those that might appear in paleoclimatological datasets. Finally, each series was re-sampled randomly 110 times, consistent with the temporal frequency of sub-samples analyzed from many Holocene sediment cores. A second, comparable dataset with a "signal" was generated by selecting one of the random series to serve as a pseudo-signal and averaging it with each

of the other 999 individual random series. The result produces a second set of time series that contain 50 % signal and 50 % random variation, which aim to mimic the noisy appearance of any real cen–mil variations in a set of paleoclimate records; i.e., these time series contain a "real" shared signal, but it is partially obscured by cen–mil noise.

3 Results

3.1 Characteristics of simulated random variation

Simulating random time series and then smoothing over 500-year windows and re-sampling at intervals consistent with paleoclimatologic records produces time series with cen–mil variation similar to that observed in many Holocene datasets (Fig. 2a, particularly if long trends were added to these series). The random data series include eye-catching, but spurious, alignments of variations (e.g., negative correlations in the bottom two series; Fig. 2a) and illustrate two important features that may serve as null expectations for evaluating actual paleoclimate time series. First, averages of multiple records (such as the six shown in Fig. 2a) produce time series with small amplitudes of variation compared to the individual time series because the random fluctuations interfere with each other. The ratio of the standard deviation of the mean time series (bold, Fig. 2a) and that of 1000 individual random series ranges from 0.27–0.41 (median 0.33) because the individual series have larger standard deviations than the dampened means when random variations cancel each other in the mean. Second, Pearson's correlation coefficients (r) among the random time series center around zero; in this example, the 95 % distribution of 1000 simulated time series equaled −0.29 to 0.30.

When a signal is incorporated into the simulated series by averaging the random variations and a common set of fluctuations (Fig. 2b), the results differ from the two null expectations as follows: (1) multi-record means retain a similar apparent amplitude of variation compared to the individual datasets (standard deviation ratio > 0.5), and (2) most of the correlations among individual time series fall outside the random distribution. The six-record mean in Fig. 2b preserves a ratio of standard deviations equal to 0.66–0.97 (median: 0.77) and correlates well ($r = 0.96$) with the introduced signal (which is the lowermost record for both panels in Fig. 2).

The simulated mean illustrates the potential for averaging ensembles of records to help retrieve weak signals which are difficult to discern in individual records. Reconstructions, particularly those averaged across sites, reduce the amplitude of any cen–mil signals (as demonstrated by standard deviation ratios < 1 in Fig. 2b), but averages of multiple records help to reduce random noise and enhance the correlation between the true signal and the ensemble reconstruction ($r > 0.5$ in Fig. 2b but < 0.4 in Fig. 2a). By contrast, noise introduced into each of the individual time series confounded the signals. For example, two event peaks at ca. 5500 and 4500 years in the "signal" do not appear in all of the series in Fig. 2b, and the absence of one versus the other can create a misleading assessment of a single asynchronous event, depending on the records used. The ensemble mean, however, successfully represents the underlying signal with both peaks (compare the bottom two curves in Fig. 2b).

3.2 Long-term Holocene trends

In the actual paleoclimate record from within and around North America, both temperature (red, Fig. 3) and moisture (blue, Fig. 3) express long-term trends, although the trends differ by scale, geographic location, season, and climate variable. The waning presence of the ice sheets and their meltwater effects on Atlantic heat transport drove early Holocene warming of > 1.5 °C (Dyke, 2004; Shuman and Marsicek, 2016), leading to summer temperature maxima from 8000–5500 yr BP. Annual temperatures (MAT) did not peak until after 5500 yr BP (Fig. 3a) because of the interacting roles of greenhouse gas and winter insolation forcing. Consistent with seasonal insolation forcing (Berger, 1978) and climate model output that demonstrates multi-millennial differences in the timing of temperature maxima based on specific temperature variable considered (Marsicek et al., 2018), sea surface and lake water temperatures (Fig. 3b) and mean temperatures of the warmest month (MTWM, Fig. 3c) peaked earlier in the Holocene than MAT. The timing of the summer maximum also varied by sub-region (Fig. 3e, g), in part because of the role of added cen–mil variability. Average water temperatures (gray, Fig. 3b) show a distinct long-term trend because of anomalous Holocene cooling in both alkenone (marine) and chironomid (lake) records, particularly near the western Atlantic (Marsicek et al., 2018; Sachs, 2007); the cooling trends in the water temperatures produce lower temperatures today than during the Younger Dryas (Fig. 3b) and generate the contrast with other datasets and simulations known as the "Holocene Temperature Conundrum" (Liu et al., 2014).

Moisture availability also includes long trends with most areas experiencing higher effective moisture in the late-Holocene than at other times (Fig. 3d, f, h). The Mid-Holocene was dry in most areas, but the influence of the Laurentide Ice Sheet before ca. 8000 yr BP enhanced moisture availability in central North America (Fig. 3f) and suppressed it substantially along the NE coast (Fig. 3h) (Shuman and Marsicek, 2016). As a result of the opposing directions of regional change, the average moisture available across all of mid-latitude sites remained intermediate until after 5500 yr BP when it rose sharply toward the present (Fig. 3d). Cen–mil variation modified these trends in different ways in different areas.

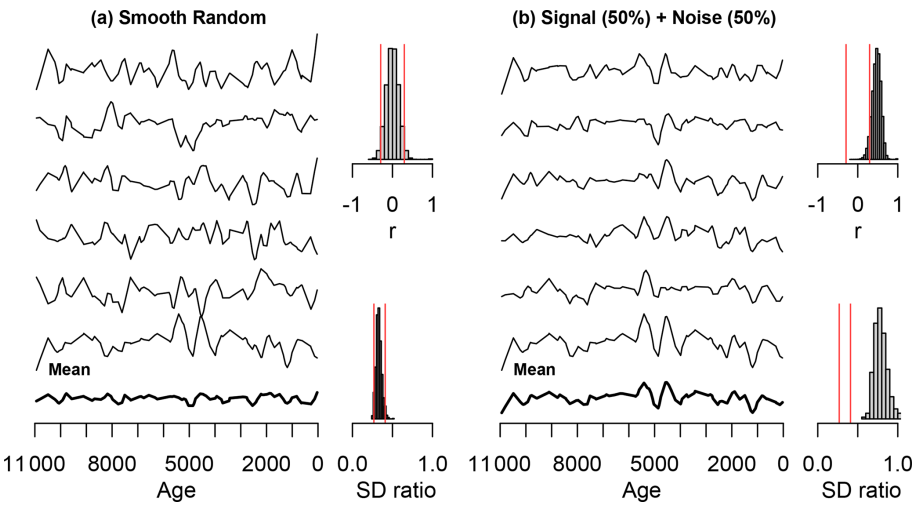

Figure 2. Simulated time series representing **(a)** six white noise series that have been smoothed to produce spurious oscillations with ∼ 500-year periods and **(b)** six series as in panel **(a)** but where the random series has been averaged with a common signal taken from the lowermost series in panel **(a)**. Bold lines at the bottom represent the means of the six series in each case. Histograms show (at the top) Pearson's product moment correlation coefficients, r, between the means and 1000 similarly generated random **(a)** or non-random **(b)** time series and (at the bottom) the ratio of the standard deviation (SD) of each mean and each of the 1000 simulated series. Red lines show the 95 % distributions of the values for the random series.

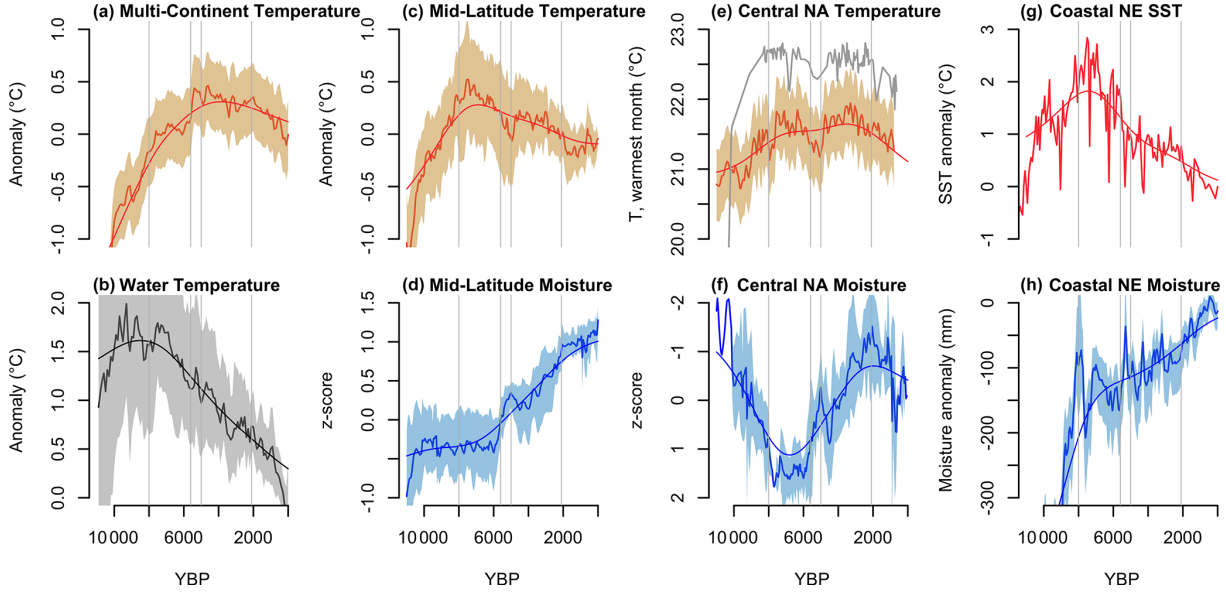

Figure 3. Holocene paleoclimate time series spanning from multi-continent to local scales representing **(a)** European and North American mean annual temperatures (MAT) (Marsicek et al., 2018), **(b)** water temperatures from the same region (Marcott et al., 2013; Marsicek et al., 2018), **(c)** mid-latitude North American mean temperatures of the warmest month (MTWM) (Shuman and Marsicek, 2016); **(d)** mid-latitude hydroclimate indicated by lake level and dust records (Shuman and Marsicek, 2016); **(e)** central North American MTWM records (Shuman and Marsicek, 2016); **(f)** central North America hydroclimate (dust) records (Dean, 1997; Nelson and Hu, 2008; Shuman and Marsicek, 2016); **(g)** alkenone-inferred SST from the Scotian Margin, core OCE326-GGC30 (Sachs, 2007; detrended as in Shuman and Marsicek, 2016); and **(h)** effective precipitation estimated from the lake level history of New Long Pond, Massachusetts (Newby et al., 2014). In panel **(e)**, the individual MTWM reconstruction from Sharkey Lake, Minnesota (Fig. 1b), is shown (black line) for comparison with the mean of the central sub-region. Vertical lines denote 8000, 5600, 5000, and 2100 yr BP. Smooth lines represent a Gaussian smoother used to detrend the records.

3.3 Patterns of cen–mil variation

Cen–mil variations rarely departed significantly from the long trends with respect to reconstruction uncertainties in the eight time series examined here (Fig. 3); detrended series remain near zero throughout the Holocene (Fig. 4). Detrended temperatures vary only 0.25–0.5 °C, which is consistent with Common Era fluctuations (PAGES 2k Consortium, 2013). The rarity of significant anomalies affirms the weak signal-to-noise ratio at cen–mil scales.

Several notable exceptions are apparent, however. A Mid-Holocene wet phase from 5600–4500 yr BP is the most prominent anomaly. It departs significantly from the mean trends in the mid-latitude, central, and northeastern coastal moisture reconstructions (Fig. 4b–d), although the duration only extends from 5500–5000 yr BP along the northeastern coast (Newby et al., 2014). Additional multi-century departures appear at 900–700 yr BP in the central moisture ensemble (Fig. 4c) and at 4400–4200 and 3400–3100 yr BP in the northeastern coast (Fig. 4d). (Note that the features recorded in the northeastern coast have been replicated in multiple reconstructions; they are not specific to the site or method (Shuman et al., 2019) and are confirmed by detailed radiocarbon dating across multiple cores and sites (Newby et al., 2014; Shuman and Burrell, 2017)).

Given the small magnitude of most cen–mil variations, correlations among the independent datasets provide support for the rigor of the signals (scatterplots, Fig. 4; Table 1), but not all of these correlations are significant compared to null distributions (Fig. 5). The strongest correlation among two independent time series of cen–mil residuals comes from the mid-latitude scale (Fig. 4b). One time series representing this scale derives from fossil pollen (MTWM; Fig. 4b) and the other from sedimentary evidence of lake level and dust deposition changes (moisture z scores; Fig. 4b). Despite the different methods and lakes involved, both mid-latitude datasets represent overlapping geographical distributions (Fig. 1b) and have large, if not significant, departures from the mean trends at 5600–4500 and 2100–750 yr BP (as well as at 10 700–9200 yr BP, which is apparent in Fig. 3b). Brief departures of the opposite sign appear centered at 750 yr BP in both series (Fig. 4b). Pearson's product–moment correlation between the two ensembles equals −0.60 (95 % range from −0.42 to −0.73; Table 1), and the correlations exceed those of random surrogates at timescales of 300–1600 years (Fig. 5b). Cooling coincides with moistening at this scale (Fig. 4).

In the coastal northeastern sub-region, the cen–mil variation in the SST and lake level records also correlate significantly (Fig. 4d). Both include repeated multi-century cool and wet fluctuations, particularly at 5500–5000, 4400–4200, 3400–3100, 2100–1300, and 1200–0 yr BP. These events alternate with warm and dry departures from the long trend at 4900–4600, 4200–3900, 2900–2100, and 1300–1200 yr BP (Newby et al., 2014; Shuman and Marsicek, 2016). Pearson's product–moment correlation coefficient ($r = -0.51$; 95 % range from −0.66 to −0.31; Table 1) and the slope of the generalized least squares model (-36 ± 8 mm °C^{-1}) both differ significantly from zero (Fig. 4d). The correlations are significant compared to those among random surrogate time series at timescales of 100–600 years (Fig. 5d).

At the scale of the central sub-region, the cen–mil correlation between temperature and moisture is weakest (Figs. 4c, 5c). Both ensembles record a large departure from the long-term trends at 5600–5000 yr BP, but the other features of the residual series are not correlated (scatterplot; Fig. 4c). Pearson's product–moment correlation coefficient ($r = -0.16$; 95 % range from −0.38 to 0.08) does not differ significantly from zero, although the slope of the generalized least squares model does ($-0.64 \pm 0.22\,z$ °C^{-1}) (Fig. 4c; Table 1). The multi-continent-scale comparison of MAT and water temperatures (Fig. 4a) also includes correlations that at first appear significant (Table 1), but they are not greater than expected from the range of surrogate random time series (Fig. 5a).

3.4 Spectral analyses

Multitaper spectral analyses of the detrended time series (Fig. 4) show that maximum spectral power exists at the scale of multiple millennia for most of the scales, regions, and variables (Fig. 6). The multi-continent spectra based on land and water temperatures both indicate increasing power from 500- to 5000-year periods, as do the spectra representing the mid-latitude region and central sub-region, which both include substantially more power at near-2000-year (4000–1500 years) periods than in the multi-century band. The slopes of the power law relationships fits to most of the spectra, which are based on z scores for comparability across variables, range from 1–2, which is 2–4 times steeper than the slopes from the NE coast (Fig. 6).

The spectra from the NE coastal sub-region differs from the others, but the temperature and moisture spectra from the sub-region are like each other (Fig. 6). Both contain peaks in power at 500-year periods, which is a timescale of variation evident in the physical stratigraphy of lakes in the region (Newby et al., 2014) and is consistent with the 100–600-year timescale of the significant correlations between the SST and lake level records (Fig. 5d). The resulting spectral slope of the z scores is low ($\sim$ 0.6–0.4) because the NE coastal records show greater power in the multi-century band and less power at multi-millennial scales than the mid-latitude region overall and central sub-regions. Thus, the coastal region expresses a higher frequency of variability in the cen–mil bands than the continental areas and larger spatial scales considered here.

3.5 Mid-Holocene changes with north–south differences

The differences across spatial scales and regions (Fig. 4) raise the question of the spatial patterns involved. The full

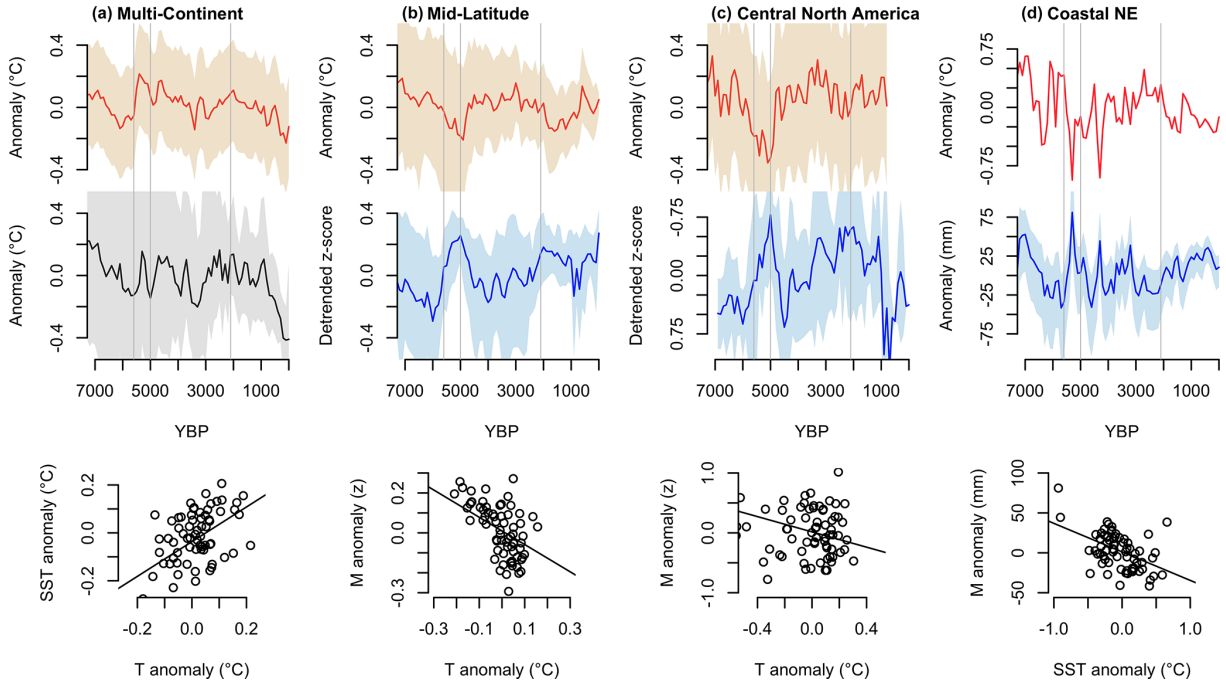

Figure 4. The same paleoclimate time series as in Fig. 3 are shown after detrending. Vertical lines in the upper panels mark 8000, 5600, 5000, and 2100 yr BP. Scatterplots show the correlations of each pair of cen–mil residuals for each scale or region over the past 7000 years. Lines in the scatterplots represent generalized least square models, which account for temporal autocorrelation. "M" indicates moisture on the y axes, and "T" is for temperature on the x axes of the scatterplots.

Table 1. Pearson product moment correlations and generalized least squares model slopes, their confidence intervals (CIs) (95 %), and timescales when the correlations exceed 95 % of random surrogate time series.

	Original citation	r	97.5 % CI	2.5 % CI	Model slope (95 % CI)	Significant timescales (yrs)
Multi-continent scale						
Mean European and North American annual temperatures (°C)	Marsicek et al. (2018)					
Mean water temperature (°C)	Marcott et al. (2013)					
	Detrended	0.57	0.71	0.38	0.72 ± 0.17 °C °C^{-1}	none
Mid-latitude eastern North America						
Mean temperature of the warmest month (°C)	Shuman and Marsicek (2016)					
Mean moisture index (z score)	Shuman and Marsicek (2016)					
	Detrended	−0.60	−0.73	−0.42	-0.68 ± 0.18 z °C^{-1}	300–1600
Central North America						
Mean temperature of the warmest month (°C)	Shuman and Marsicek (2016)					
Mean moisture index (z score)	Shuman and Marsicek (2016)					
	Detrended	−0.16	−0.38	0.08	-0.64 ± 0.22 z °C^{-1}	none
Northeast coastal North America						
Uk'37 sea surface temperature, OCE326-GGC30 (°C)	Sachs (2007)					
Effective precipitation departure from present estimated from lake level change, New Long Pond, Massachusetts (mm)	Newby et al. (2014)					
	Detrended	−0.51	−0.66	−0.31	35 ± 0.7 mm °C^{-1}	100–600 years

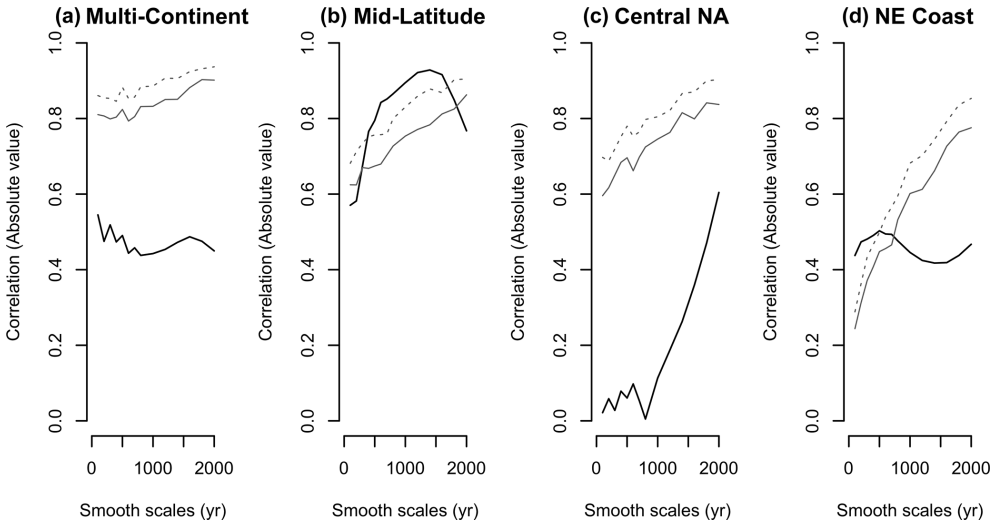

Figure 5. Timescale-dependent correlations for the four spatial scales over the past 6000 years. Black lines show the correlations (as absolute values) between the two detrended paleoclimate time series for each scale or region (as shown in Fig. 3) after Gaussian filtering using cut-off frequencies of $1/t$, where t (smoothing scale) ranges from 100–2000 years; gray lines show the 90 % (solid line) and 95 % (dashed line) correlations for 1000 surrogate random time series generated as power law time series with the same spectral slope as the paleoclimate reconstructions using the GenNullHypPair function in the corit package (Reschke et al., 2019).

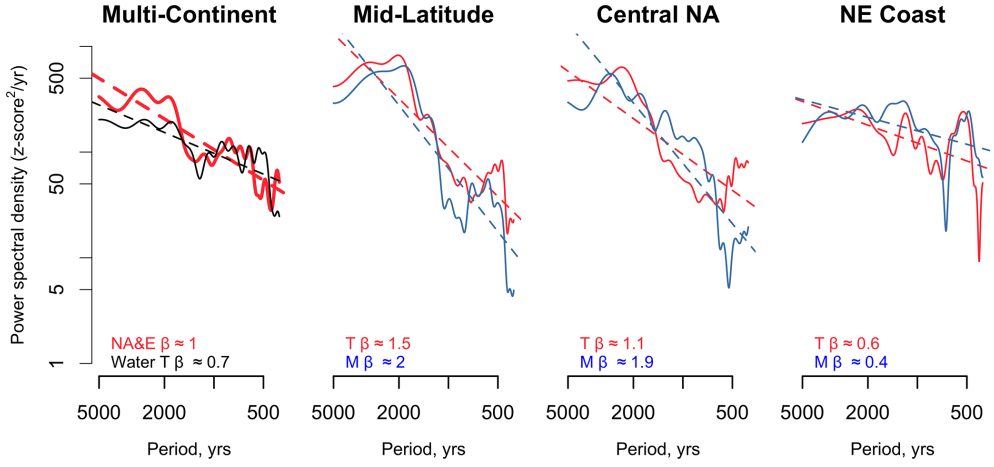

Figure 6. Multitaper spectral density plots show each time series of detrended cen–mil residuals in Fig. 3, represented as z scores to enable direct comparison within each pair of independent time series, with respect to log spectral power and period. Beta values represent the slope of the power law relationship fit to the data. Red curves represent temperature (T) time series, and blue curves represent moisture (M). Slopes shown here were fit over periods from 5000–400 years.

ensemble of MTWM reconstructions from mid-latitude sites (Shuman and Marsicek, 2016) enables further evaluation of the most prominent cen–mil feature of the different ensembles, which is the significant Mid-Holocene anomaly from ca. 5600–5000 yr BP (Fig. 4). To aid the analysis of this anomaly, the MTWM ensemble can be subdivided according to records that warmed or cooled after the event, which was determined here by subtracting the mean post-event temperature from 4700–4100 yr BP from the mean temperature when the anomalies first developed (5600–5000 yr BP; Fig. 7). If the temperature difference across these two periods was arbitrary, then the time series of temperature changes from the warming and cooling regions might expect to show a slow change (i.e., some sites might change early compared to the 600-year windows and others might change later; some may change slowly and others fast). Instead, rapid changes between 5200–4700 yr BP appear in individual records (see e.g., Shuman et al., 2023), the two subset means (thick lines with uncertainty; Fig. 7a), and temperature-sensitive geochemical records from the two regions (thin lines, Fig. 7a) (Puleo et al., 2020; Henne and Hu, 2010). The two subsets correlate with each other ($r = 0.48$), but other than the rapid changes at 5200–4700 yr BP, the cen–mil features of the two time series are not correlated.

The pattern of change reflects a steepening in the north–south temperature gradient at ca. 5200–4700 yr BP (Fig. 7), which additional sites in the northeastern USA confirm, plausibly also including early cooling in the north before warming in the south (Shuman et al., 2023). However, the mapped changes (Fig. 7b) indicate that the steepening of the temperature gradient was not limited to the northeastern US. Across the whole mid-latitude region, pairs of sites from different latitudes at any given longitude tend to show rapid warming at the southern site and cooling at the northern site (Fig. 7b). However, the boundary between areas of warming and cooling does not follow a fixed latitude but curves across the region as develops today in response to the North Atlantic Oscillation (NAO) (Shuman et al., 2023; Folland et al., 2009) (shading; Fig. 7b). The change also extends beyond the region of a coincident and widespread decline in hemlock (*Tsuga*) pollen percentages, which includes Ontario and the northeastern US (Foster et al., 2006; Bennett and Fuller, 2002) but not the Minnesota, Wisconsin, or other central subregion records used here. In the northeastern US, a deviation from the north–south pattern produced a strong coastal–inland contrast of coastal cooling versus inland warming (Marsicek et al., 2013) (Fig. 7b), which is consistent with expected SST changes and resulting coastal cooling on land (Shuman et al., 2023).

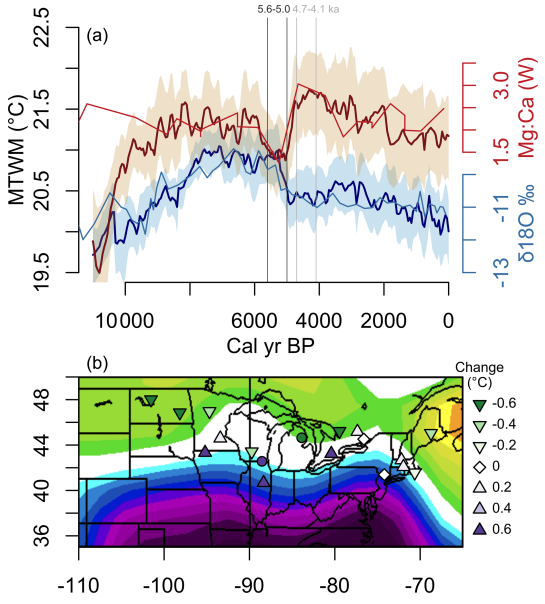

Figure 7. **(a)** The average time series of mean temperature of the warmest month (MTWM) from sites that either warmed in the Mid-Holocene after a cool millennium (red) or cooled after a warm period (blue) are shown along with example temperature-sensitive geochemical records (thin lines) from each region, including a reconstruction of water (W) Mg : Ca from Lake Geneva, Wisconsin (purple circle in panel **b**) (Puleo et al., 2020), and carbonate oxygen isotope ratios from O'Brien Lake, Michigan (green circle in panel **b**) (Henne and Hu, 2010). The 50 % range of 100 possible 5-site averages of the MTWM reconstructions is shown as the shaded uncertainty for each series. **(b)** Mapped triangles show the locations of warming (upward triangles) and cooling (downward triangles) based on the differences in the mean temperatures from 5600–5000 and 4700–4100 yr BP (denoted by gray and black lines in panel **(a)** and labeled using ages in thousands of years or ka). Green shading reflects the magnitude of cooling; purple shows the magnitude of warming. Underlying contours indicate historic (1948–2015 CE) correlations between June–August mean temperatures and the North Atlantic Oscillation index from https://www.psl.noaa.gov/data/correlation/ (last access: 1 October 2023); shades of green and purple show positive and negative correlations, respectively, up to 0.4.

4 Discussion

4.1 Patterns of cen–mil variability

Holocene paleoclimate reconstructions spanning a range of scales from multiple continents to individual sites contain evidence of cen–mil variation within the past 7000 years, after dynamics related to ice sheets and meltwater were no longer significant (Fig. 4). The temperature variations were small (< 0.25 °C), which challenges detection, especially compared to the confidence intervals of the reconstructions (Figs. 3–4). However, reconstruction uncertainty incorporates errors associated with reconstructing absolute temperatures, which may not apply to the relative, detrended

changes examined here. Furthermore, some of the temperature variations correlate well with independent moisture datasets (Figs. 4–5). The consistency is greater than expected from random variations (Fig. 5), appears evident in the frequency and time domain (Fig. 6), and highlights two prominent patterns of cen–mil variation.

First, at the regional scale, mid-latitude MTWM (top, Fig. 4b) and mid-latitude hydroclimate reconstructions (bottom, Fig. 4b) share a correlated pattern of multi-millennial variation (Fig. 5) with spectral power centered at periods around 2000 years (Fig. 6). The broad spectral peak confirms that the variations are not cyclical but produced mid-latitude temperature minima at 5600–5000 and after 2100 yr BP (Fig. 4b), which are also evident in both the central (Fig. 4c) and coastal sub-regions (Fig. 4d). The pattern propagates down to the scale of individual central sites such as Sharkey Lake, Minnesota (black line; top, Fig. 3e). The cool phases coincide with high moisture levels at 5600–5000 and after 2100 yr BP, which represent significant departures (non-zero anomalies) from the long-term moisture trends in both the mid-latitude mean (Figs. 3d, 4b) and the NE coastal reconstruction (Figs. 3h, 4d). At least some of the temperature variation appears as a north–south anti-phased pattern across the mid-latitude region (Fig. 7), which bears some similarities to the summer NAO at interannual timescales (Fig. 7b). The most pronounced steepening of the temperature difference between areas that warmed or cooled at ca. 5200–4700 yr BP (after the prominent anomaly from 5600–5000 yr BP) developed from ca. 4800–3800 yr BP (Shuman et al., 2023), possibly indicating different millennial-length phases of negative versus positive NAO states. Whether the phases represent changes in the frequency of interannual NAO modes or millennial-scale variations analogous to, but much slower than, the interannual oscillation is unclear. The pattern has similarities to those detected during the Younger Dryas (Fastovich et al., 2020), but the correlations among temperatures and moisture at cen–mil scales (Fig. 4) differ from the temperature–moisture relationships in the long Holocene trends (Fig. 3), indicating that different processes were likely involved.

Second, ∼350-year variability appears superimposed on the broad-scale variations along the northeastern coast (Figs. 4–6). The northeastern SST reconstruction correlates with the drought history along the coast (Fig. 4d), particularly over 100–600-year scales (Fig. 5d), but the high-frequency (multi-century) variations appear weaker in most other regions (Fig. 6). A network of northeastern lake level records also shows evidence of both the millennial pattern evident at the mid-latitude-scale and the additional multi-century variability (Newby et al., 2014; Shuman and Burrell, 2017), although the spatial patterns differ from each other and may confirm two superimposed dynamics. The widely prominent event from 5600–5000 yr BP includes a strong east–west contrast but repeated warm–dry events at 4900–4600, 4200–3900, 2900–2100, and 1300–1200 yr BP do not (Newby et al., 2014; Shuman and Burrell, 2017; Shuman and Marsicek, 2016). Here, the patterns are detected using independent sets of lakes and cores (i.e., the pollen-inferred temperatures do not derive from the same lakes as the moisture histories).

The first pattern may be stronger at regional scales across mid-latitude North America than across the larger multi-continent scale represented by the MAT reconstruction (Figs. 3a, 4a) because related variations in the different sign cancel at the largest scales. The multi-continent MAT and water temperatures include many records in the eastern Atlantic and European regions (Fig. 1a), which may include different influences and expressions; the mid-latitude reconstructions likely emphasize variations common at the scale of westerly waves or other synoptic features, which cancel across regions at the multi-continent scale. The multi-continent MAT record includes a step shift at 5600 yr BP (Fig. 3a), which may be related to the prominent mid-latitude anomaly at 5600–5000 yr BP (Fig. 4), but sub-regional subsets that represent inland versus coastal areas (Fig. 4C-D) or northern versus southern areas (Fig. 7) highlight the added geographic differences.

In central North America, cen–mil variation appears weaker and less consistent than in other areas (Figs. 4–5). Potentially, teleconnections and interactions in this region may be more variable than in other areas, such as the northeastern coast. The difference is analogous to different teleconnected responses to tropical Pacific and North Atlantic variability today, which have more consistent responses to interannual variability in some areas than others.

4.2 Mid-Holocene anomaly

The most significant anomaly in many records falls between 5600–5000 yr BP (Figs. 3–4). Qualitative evidence of a "Mid-Holocene anomaly" has existed for decades in North America. At Elk Lake, Minnesota, the varve record contains a phase of reduced dust deposition and varve thicknesses (Dean, 1997). Fossil pollen records from the Great Plains, such as Creel Bay, Spiritwood, and Moon lakes in North Dakota and Pickerel Lake in South Dakota, contain a conspicuous interval of low *Ambrosia* (ragweed) pollen (Grimm, 2001), while unique ostracod assemblages at 5600–5000 yr BP indicate severe drought in Minnesota (Smith et al., 2002). Lake level records in the Rocky Mountains indicate a distinct phase of high water in Wyoming and Colorado (Shuman et al., 2014; Shuman and Marsicek, 2016), while those in inland areas of the northeastern US record low water at the same time (Newby et al., 2011; Shuman and Burrell, 2017). Submerged tree stumps within Lake Tahoe, California, date to this interval (Benson et al., 2002), which also includes anomalies in other regions (Magny et al., 2006; Magny and Haas, 2004), such as the Mediterranean Sea (Alboran cooling event 2; Cacho et al., 2001; Fletcher et al., 2013) and Africa (Berke et al., 2012; Thompson et al., 2002).

A similar Mid-Holocene anomaly has been widely recognized across the North Atlantic region. Records document shifts in deep water from 5500–4700 yr BP (Oppo et al., 2003) and other distinct anomalies from the Labrador to Norway in sea surface temperatures, salinity, loess, and precipitation (Giraudeau et al., 2010; Jackson et al., 2005; Larsen et al., 2012; Orme et al., 2021). An earlier dust accumulation anomaly on the Greenland summit, interpreted to represent a shift in atmospheric circulation from 6000–5100 yr BP, may be related to these patterns (Mayewski et al., 2004). Likewise, a negative phase of the NAO may be consistent with distinct and contrasting phases of anomalous warmth on the Labrador Shelf from 5700–4800 yr BP (Lochte et al., 2020) and cold in the Florida Strait from 5500–4400 yr BP (Schmidt et al., 2012). The weak latitudinal temperature gradient before the transition at ca. 5000–4700 yr BP was followed by a steep gradient until ca. 3500 yr BP, particularly in the northeastern US and the adjacent Atlantic (Shuman et al., 2023), and could be consistent with either a shift from negative- to positive-dominated NAO regimes or an analogous low-frequency change in the Atlantic pressure field. However, the sign of the NAO analog may depend upon whether the patterns detected here represent mean annual or summer temperature shifts (contrast Fig. 7b with similar maps for mean annual anomalies in Shuman et al., 2023).

The Mid-Holocene anomaly from 5500–5000 yr BP, like a possible anomaly of the opposite sign after 4800 yr BP (Fig. 7b) (Shuman et al., 2023), would not be expected to appear in all records or regions. Spatial heterogeneity in detecting the pattern would be consistent with the small magnitude of cen–mil variations (Fig. 4), interactions with other trends (Fig. 3), and the inherent spatial variability in such dynamics (Fig. 7). In some areas, the millennial-scale variation could at first delay and then reinforce the direction of the long-term trends producing a step change (e.g., northern sites in blue in Fig. 7a). Such a step-like cooling pattern may extend across eastern Canada and northern and eastern Greenland, which could be consistent with NAO-like outcomes in annual temperatures (Briner et al., 2016; Shuman et al., 2023). Only in some areas, where the millennial variation temporarily counteracted the long trends, would the anomaly be expressly apparent without detrending (e.g., southern sites in red in Fig. 7a; moisture variations in central North America in Fig. 3f).

4.3 Potential drivers

The dynamics driving the two patterns of cen–mil variation here (broad-scale millennial variations including at 5500–5000 yr BP and northeastern coastal multi-century variations) need further investigation. As noted above, the north–south differences across mid-latitude sites may indicate a role of variability in the Atlantic pressure gradient similar to the NAO at monthly to interannual timescales. NAO-like dynamics may be expressed at cen–mil scales (Olsen et al., 2012; Orme et al., 2021; Shuman et al., 2023) and are usually strongest in winter, but they can have an important form of expression in summer, extending from North America to Europe (Folland et al., 2009). The prominence of the Mid-Holocene shift in the mid-latitude records examined here (Figs. 6–7) and elsewhere (Willard et al., 2005) also raises the question of whether the change originated from other feedbacks that affect Atlantic sector pressure gradients such as by altering the depth of the African monsoon low (Claussen et al., 1999), potentially via dust loading feedbacks (Pausata et al., 2016), or whether millennial-scale variation interfered with long trends to produce state shifts on multiple continents at approximately the same time. For example, northern cooling by ca. 4700 yr BP (Fig. 7), which may reflect NAO-like dynamics that began as early as 6200 yr BP in some areas (Shuman et al., 2023), could have been a driving factor in the chain of dynamics that produced rapid changes to the African monsoon system (Collins et al., 2017). Resulting feedbacks may then have reinforced the abrupt changes at mid- and high latitudes (Muschitiello et al., 2015) (Fig. 7).

The multi-century variability expressed along the Atlantic coast also has similarities to variations observed in other Atlantic sectors, including off the West African coast (Adkins et al., 2006; deMenocal et al., 2000) and the Mediterranean (Fletcher et al., 2013). Holocene simulations indicate Atlantic–African–American linkages should be expected (Muschitiello et al., 2015). These sectors may be linked via the dynamics of the North Atlantic subtropical high (Clement et al., 2015), possibly driven by cloud feedbacks (Bellomo et al., 2016), atmospheric feedbacks on meridional overturning (Wills et al., 2019), or volcanism (Birkel et al., 2018; Kobashi et al., 2017); similar dynamics on interannual scales have consequences for North American hydroclimate patterns (Enfield et al., 2001; Anchukaitis et al., 2019).

A preliminary comparison of alkenone records from the Scotian and Virginia margins (Sachs, 2007) and the West African margin (Adkins et al., 2006) reveal that they potentially share a multi-century pattern of variability over the past 6000 years, which is expressed by different sign changes between Scotian and African margins with the sign of the variation switching between early and late events off Virginia (Fig. 8). Principal component (PC) analysis indicates that, at face value and given current age control, the pattern represents 11 % of the variance within the three records over the past 8000 years but 23 % in the past 6000 years. (The first PC represents 72 % of the variance and the long-term trend over the past 8000 years). The multi-century SST variability correlates with the coastal hydroclimate variability (Fig. 8) and may also involve shifts in the temperature gradient over the western Atlantic and Greenland (Shuman et al., 2019). However, the multi-century SST and hydroclimate variability along the western Atlantic margin does not extend to similar large-scale temperature gradient changes (Fig. 7). Therefore,

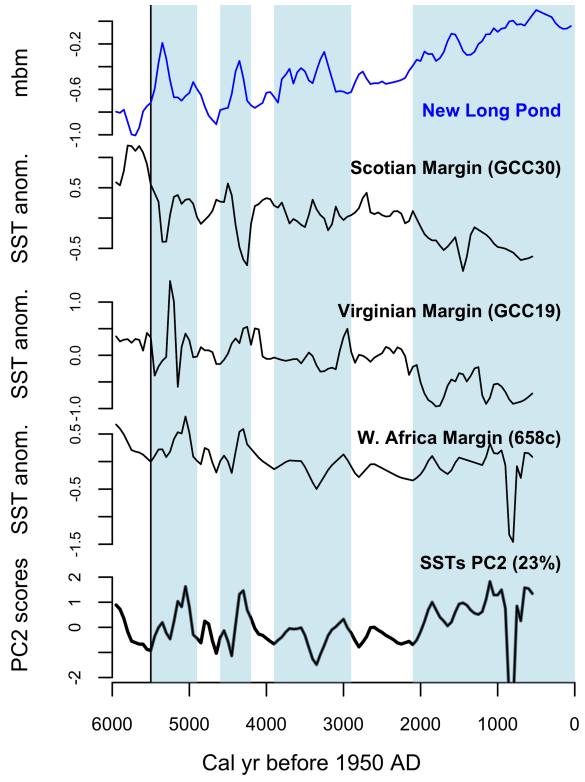

Figure 8. Comparison of the lake level record from New Long Pond, Massachusetts (Fig. 3h), and three alkenone-inferred sea surface temperature (SST) records (Adkins et al., 2006; Sachs, 2007). The SST records are shown after detrending and with the second principal component (PC2) scores of a principal component analysis conducted on the non-detrended series; the first PC captures the trends. Blue bands represent the timing of wet phases identified from radiocarbon-dated paleo-shorelines at multiple lakes in coastal Massachusetts (Newby et al., 2014). The term "mbm" refers to meters below modern water level.

at least two different dynamics, even if they are different seasonal expressions of NAO-like variations, must be involved.

4.4 Signal detection

Cen–mil variability is small relative to the ability to detect it. Several factors may aid efforts to examine these dynamics. First, analyses of calibrated rather than relative paleoclimate records may aid detection if all records involved in an analysis capture the variations in similar, linear ways (e.g., tree rings, Anchukaitis et al., 2019; pollen, Shuman et al., 2023; marine geochemical records, Osman et al., 2021). For example, calibration of fossil pollen using the modern analog or similar techniques removes inherent non-linearities in the responses of individual plant taxa and isolates the effects of focal climate variables from the interacting influences of other factors. While the responses of individual taxa are non-linear, the calibrated pollen assemblage (plant community) response is likely to be linear (Shuman et al., 2019). Other calibrated indices, such as chironomid- or alkenone-derived temperatures, should behave similarly, although relative paleoclimate indices may be more complex (Axford et al., 2011). Relative indices may be particularly problematic if they are not multi-variate and only shift in a bivariate fashion with respect to a wide range of different influences (e.g., sediment carbon : nitrogen ratios and stable isotopes). For example, some isotope data series may not be meaningfully different from random noise in some settings if multiple competing influences, such as temperature, air mass trajectories, precipitation seasonality, evaporation, and groundwater inputs, interact to create complex signals (e.g., Donovan et al., 2002; Steinman et al., 2010). However, systematic treatment of stable isotopic datasets based on their relationship to the locally dominant driving processes can avoid this type of problem (Konecky et al., 2023).

Second, ensembles of detailed, well-dated records from the same climatic region or scale increase the likelihood that noise can be removed through averaging (Fig. 2) (Konecky et al., 2023; Shuman et al., 2023), although doing so may also reduce the amplitude of the cen–mil variations (SD ratios < 1 in Fig. 2b) (Hébert et al., 2022). Such ensembles may need to be created and analyzed in a manner that accounts for (a) the potential that different climate variables or regions can change asynchronously at the beginning and ends of events (Fig. 7a) (Rach et al., 2014; Gonzales and Grimm, 2009; Ma et al., 2012) and (b) different expressions of the same events in different regions or sub-regions (Fig. 7b) (Shuman et al., 2023; Fastovich et al., 2020). These issues can be resolved using cluster analyses or similar techniques to subdivide potential sets of records (Shuman et al., 2023) and focusing on time series correlation, especially compared to surrogates (Reschke et al., 2019), or the temporal overlap of full events rather than precise synchrony of the abrupt changes that bound them (Parnell et al., 2008; Newby et al., 2014).

Third, comparisons of independent ensembles of data from the same area allow the signals to be cross-validated. Analyses here benefitted from ensembles based on many cores (> 600 fossil pollen records, > 30 cores across 9 lake level study sites, and dozens of water temperature records) which reduced age and reconstruction uncertainties. The different ensembles of temperature and moisture were also developed in fundamentally different ways (e.g., microfossil versus physical sedimentological analyses), which indicated that any shared signals had a broad basis of evidence indicating multivariate environmental responses to even weak climate fluctuations. Finally, and even in the absence of the above criteria, comparisons of paleoclimate reconstructions with random surrogate datasets (Fig. 5) provide a powerful tool for distinguishing between spurious and significant variations (Fig. 2) (Reschke et al., 2019; Telford and Birks, 2011).

5 Conclusions

In areas centered on mid-latitude eastern North American, coherent cen–mil variation has similar signal magnitudes in independent temperature and hydroclimate datasets. The major signals, including prominent Mid-Holocene anomalies from 5600–5000 yr BP, are not readily falsified using the analyses here because they share the characteristics of non-random signals. The variations played important roles in mediating long-term trends, creating differences in the timing of the Holocene thermal maximum and rates of early-Holocene warming and late-Holocene cooling among regions. Events that have previously attracted focused attention, such as at 9300, 8200, 4200, and 2700 yr BP, do not stand out as the most distinct features of the ensembles of data compiled here.

Instead, two major patterns of variability appear evident. One appears expressed across a broad range of spatial scales, which is similar to some unforced global variability in transient climate simulations (Marsicek et al., 2018; Wan et al., 2019). The pattern includes a set of millennial fluctuations with important anomalies and rapid shifts in both temperature and moisture gradients at ca. 5000 and 2100 yr BP. More work is needed to evaluate whether such broad-scale changes, including Mid-Holocene anomalies, stem from external forcing, such as solar or volcanic events, intrinsic ocean or atmosphere variability, or other factors such as surface–atmosphere feedbacks, but the spatial patterns indicate that shifts in summer atmospheric pressure gradients over the Atlantic, such as associated with the NAO at short timescales, may be involved. The second major pattern produced a series of multi-century hydroclimate fluctuations along the Atlantic coast and may relate to Atlantic SST variability with distinctive spectral properties not seen in most of the study area. Because pollen and lake level records detect the events, they had ecological, hydrological, geomorphic, and, therefore, likely human significance and deserve further investigation.

Data availability. The different ensembles of data examined here are available through the NOAA National Centers for Environmental Information Paleoclimatology Database:

- North Atlantic and adjacent continental reconstructions (Marsicek et al., 2018) are available at https://www.ncdc.noaa.gov/paleo-search/study/22992.
- Mid-latitude North America and sub-regional temperature and moisture reconstructions (Shuman and Marsicek, 2016) are available at https://www.ncdc.noaa.gov/paleo-search/study/31097.
- New Long Pond, Massachusetts, USA (coastal northeastern US), lake level reconstruction (Newby et al., 2014) is available at https://www.ncdc.noaa.gov/paleo-search/study/23074.
- Scotian Margin sea surface temperature reconstruction (OCE326-GGC30) (Sachs, 2007) is available at https://www.ncdc.noaa.gov/paleo-search/study/6409.

Competing interests. The author has declared that there are no competing interests.

Disclaimer. Publisher's note: Copernicus Publications remains neutral with regard to jurisdictional claims made in the text, published maps, institutional affiliations, or any other geographical representation in this paper. While Copernicus Publications makes every effort to include appropriate place names, the final responsibility lies with the authors.

Acknowledgements. Cody Routson, Carrie Morrill, Lorelei Curtin, Dulcinea Groff, Ioana Stefanescu, Raphael Hébert, and an anonymous reviewer kindly provided thoughtful comments on the paper.

Financial support. This research has been supported by the National Science Foundation (grant nos. DEB-1856047 and EAR-1903729).

Review statement. This paper was edited by Alberto Reyes and reviewed by Raphael Hébert and one anonymous referee.

References

Adkins, J., deMenocal, P., and Eshel, G.: The African humid period and the record of marine upwelling from excess ^{230}Th in Ocean Drilling Program Hole 658C, Paleoceanography, 21, PA4203, https://doi.org/10.1029/2005pa001200, 2006.

Anchukaitis, K. J., Cook, E. R., Cook, B. I., Pearl, J., D'Arrigo, R., and Wilson, R.: Coupled Modes of North Atlantic Ocean-Atmosphere Variability and the Onset of the Little Ice Age, Geophys. Res. Lett., 46, 12417–12426, https://doi.org/10.1029/2019GL084350, 2019.

Ault, T. R., Cole, J. E., Overpeck, J. T., Pederson, G. T., George, S. S., Otto-Bliesner, B., Woodhouse, C. A., and Deser, C.: The Continuum of Hydroclimate Variability in Western North America during the Last Millennium, J. Climate, 26, 5863–5878, 2013.

Ault, T. R., George, S. S., Smerdon, J. E., Coats, S., Mankin, J. S., Carrillo, C. M., Cook, B. I., and Stevenson, S.: A Robust Null Hypothesis for the Potential Causes of Megadrought in Western North America, J. Climate, 31, 3–24, https://doi.org/10.1175/JCLI-D-17-0154.1, 2018.

Axford, Y., Andresen, C. S., Andrews, J. T., Belt, S. T., Geirsdóttir, Á., Massé, G., Miller, G. H., Ólafsdóttir, S., and Vare, L. L.: Do paleoclimate proxies agree? A test comparing 19 late Holocene climate and sea-ice reconstructions from Icelandic marine and lake sediments, J. Quaternary Sci., 26, 645–656, https://doi.org/10.1002/jqs.1487, 2011.

Bellomo, K., Clement, A. C., Murphy, L. N., Polvani, L. M., and Cane, M. A.: New observational evidence for a positive cloud feedback that amplifies the Atlantic Multidecadal Oscillation, Geophys. Res. Lett., 43, 9852–9859, https://doi.org/10.1002/2016GL069961, 2016.

Bender, M. L.: Paleoclimate, Princeton University Press, 320 pp., ISBN 9780691145549, 2013.

Bennett, K. D. and Fuller, J. L.: Determining the age of the mid-Holocene Tsuga canadensis (hemlock) decline, eastern North America, The Holocene, 12, 421–429, https://doi.org/10.1191/0959683602hl556rp, 2002.

Benson, L., Kashgarian, M., Rye, R., Lund, S., Paillet, F., Smoot, J., Kester, C., Mensing, S., Meko, D., and Lindström, S.: Holocene multidecadal and multicentennial droughts affecting Northern California and Nevada, Quaternary Sci. Rev., 21, 659–682, 2002.

Berger, A.: Long-term variations of caloric insolation resulting from the earth's orbital elements, Quaternary Res., 9, 139–167, 1978.

Berke, M. A., Johnson, T. C., Werne, J. P., Schouten, S., and Sinninghe Damsté, J. S.: A mid-Holocene thermal maximum at the end of the African Humid Period, Earth Planet. Sc. Lett., 351–352, 95–104, https://doi.org/10.1016/j.epsl.2012.07.008, 2012.

Birkel, S. D., Mayewski, P. A., Maasch, K. A., Kurbatov, A. V., and Lyon, B.: Evidence for a volcanic underpinning of the Atlantic multidecadal oscillation, NPJ Clim. Atmos. Sci., 1, 1–7, https://doi.org/10.1038/s41612-018-0036-6, 2018.

Briner, J. P., McKay, N. P., Axford, Y., Bennike, O., Bradley, R. S., de Vernal, A., Fisher, D., Francus, P., Fréchette, B., Gajewski, K., Jennings, A., Kaufman, D. S., Miller, G., Rouston, C., and Wagner, B.: Holocene climate change in Arctic Canada and Greenland, Quaternary Sci. Rev., 147, 340–364, https://doi.org/10.1016/j.quascirev.2016.02.010, 2016.

Cacho, I., Grimalt, J. O., Canals, M., Sbaffi, L., Shackleton, N. J., Schönfeld, J., and Zahn, R.: Variability of the western Mediterranean Sea surface temperature during the last 25,000 years and its connection with the Northern Hemisphere climatic changes, Paleoceanography, 16, 40–52, https://doi.org/10.1029/2000PA000502, 2001.

Camill, P., Umbanhowar Jr, C. E., Teed, R., Geiss, C. E., Aldinger, J., Dvorak, L., Kenning, J., Limmer, J., and Walkup, K.: Late-glacial and Holocene climatic effects on fire and vegetation dynamics at the prairie-forest ecotone in south-central Minnesota, J. Ecol., 91, 822–836, 2003.

Claussen, M., Kubatzki, C., Brovkin, V., Ganopolski, A., Hoelzmann, P., and Pachur, H. J.: Simulation of an abrupt change in Saharan vegetation in the mid-Holocene, Geophys. Res. Lett., 26, 2037–2040, 1999.

Clement, A., Bellomo, K., Murphy, L. N., Cane, M. A., Mauritsen, T., Rädel, G., and Stevens, B.: The Atlantic Multidecadal Oscillation without a role for ocean circulation, Science, 350, 320–324, https://doi.org/10.1126/science.aab3980, 2015.

Collins, J. A., Prange, M., Caley, T., Gimeno, L., Beckmann, B., Mulitza, S., Skonieczny, C., Roche, D., and Schefuß, E.: Rapid termination of the African Humid Period triggered by northern high-latitude cooling, Nat. Commun., 8, 1372, https://doi.org/10.1038/s41467-017-01454-y, 2017.

Crucifix, M., de Vernal, A., Franzke, C., and von Gunten, L.: Centennial to Millennial Climate Variability, Past Global Changes Magazine, 25, 131–166, https://doi.org/10.22498/pages.25.3, 2017.

Dean, W. E.: Rates, timing, and cyclicity of Holocene eolian activity in north-central United States; evidence from varved lake sediments, Geology, 25, 331–334, 1997.

deMenocal, P. B.: Cultural Responses to Climate Change During the Late Holocene, Science, 292, 667–673, https://doi.org/10.1126/science.1059287, 2001.

deMenocal, P., Ortiz, J., Guilderson, T., and Sarnthein, M.: Coherent High- and Low-Latitude Climate Variability During the Holocene Warm Period, Science, 288, 2198–2202, https://doi.org/10.1126/science.288.5474.2198, 2000.

Donovan, J. J., Smith, A. J., Panek, V. A., Engstrom, D. R., and Ito, E.: Climate-driven hydrologic transients in lake sediment records: calibration of groundwater conditions using 20th century drought, Quaternary Sci. Rev., 21, 605–624, 2002.

Dyke, A. S.: An outline of North American deglaciation with emphasis on central and northern Canada, in: Developments in Quaternary Science, edited by: Ehlers, J. and Gibbard, P. L., Elsevier, 373–424, ISBN 978-0-444-51592-6, 2004.

Enfield, D. B., Mestas-Nuñez, A. M., and Trimble, P. J.: The Atlantic Multidecadal Oscillation and its relation to rainfall and river flows in the continental U.S., Geophys. Res. Lett., 28, 2077–2080, https://doi.org/10.1029/2000GL012745, 2001.

Fastovich, D., Russell, J. M., Jackson, S. T., Krause, T. R., Marcott, S. A., and Williams, J. W.: Spatial Fingerprint of Younger Dryas Cooling and Warming in Eastern North America, Geophys. Res. Lett., 47, e2020GL090031, https://doi.org/10.1029/2020GL090031, 2020.

Fletcher, W. J., Debret, M., and Goñi, M. F. S.: Mid-Holocene emergence of a low-frequency millennial oscillation in western Mediterranean climate: Implications for past dynamics of the North Atlantic atmospheric westerlies, The Holocene, 23, 153–166, https://doi.org/10.1177/0959683612460783, 2013.

Folland, C. K., Knight, J., Linderholm, H. W., Fereday, D., Ineson, S., and Hurrell, J. W.: The Summer North Atlantic Oscillation: Past, Present, and Future, J. Climate, 22, 1082–1103, https://doi.org/10.1175/2008JCLI2459.1, 2009.

Foster, D. R., Oswald, W. W., Faison, E. K., Doughty, E. D., and Hansen, B. C. S.: A climatic driver for abrupt mid-Holocene vegetation dynamics and the hemlock decline in New England, Ecology, 87, 2959–2966, 2006.

Giraudeau, J., Grelaud, M., Solignac, S., Andrews, J. T., Moros, M., and Jansen, E.: Millennial-scale variability in Atlantic water advection to the Nordic Seas derived from Holocene coccolith concentration records, Quaternary Sci. Rev., 29, 1276–1287, https://doi.org/10.1016/j.quascirev.2010.02.014, 2010.

Gonzales, L. M. and Grimm, E. C.: Synchronization of late-glacial vegetation changes at Crystal Lake, Illinois, USA with the North Atlantic Event Stratigraphy, Quaternary Res., 72, 234–245, 2009.

Grimm, E. C.: Trends and palaeoecological problems in the vegetation and climate history of the northern Great Plains, U.S.A, Biol. Environ. Proc. R. Ir. Acad., 99B, 1–18, 2001.

Hébert, R., Herzschuh, U., and Laepple, T.: Millennial-scale climate variability over land overprinted by ocean temperature fluctuations, Nat. Geosci., 15, 899–905, https://doi.org/10.1038/s41561-022-01056-4, 2022.

Henne, P. D. and Hu, F. S.: Holocene climatic change and the development of the lake-effect snowbelt in Michigan, USA, Quaternary Sci. Rev., 29, 940–951, https://doi.org/10.1016/j.quascirev.2009.12.014, 2010.

Hernández, A., Martin-Puertas, C., Moffa-Sánchez, P., Moreno-Chamarro, E., Ortega, P., Blockley, S., Cobb, K. M., Comas-Bru, L., Giralt, S., Goosse, H., Luterbacher, J., Martrat, B.,

Muscheler, R., Parnell, A., Pla-Rabes, S., Sjolte, J., Scaife, A. A., Swingedouw, D., Wise, E., and Xu, G.: Modes of climate variability: Synthesis and review of proxy-based reconstructions through the Holocene, Earth-Sci. Rev., 209, 103286, https://doi.org/10.1016/j.earscirev.2020.103286, 2020.

Herzschuh, U., Böhmer, T., Chevalier, M., Hébert, R., Dallmeyer, A., Li, C., Cao, X., Peyron, O., Nazarova, L., Novenko, E. Y., Park, J., Rudaya, N. A., Schlütz, F., Shumilovskikh, L. S., Tarasov, P. E., Wang, Y., Wen, R., Xu, Q., and Zheng, Z.: Regional pollen-based Holocene temperature and precipitation patterns depart from the Northern Hemisphere mean trends, Clim. Past, 19, 1481–1506, https://doi.org/10.5194/cp-19-1481-2023, 2023.

Hurrell, J. W., Kushnir, Y., Ottersen, G., and Visbeck, M.: The North Atlantic Oscillation: Climatic Significance and Environmental Impact, Geophysical Monograph Series, vol. 134, American Geophysical Union, 279 pp., ISBN 9780875909943, 2003.

Huybers, P. and Curry, W.: Links between annual, Milankovitch and continuum temperature variability, Nature, 441, 329–332, https://doi.org/10.1038/nature04745, 2006.

Jackson, M. G., Oskarsson, N., Trønnes, R. G., McManus, J. F., Oppo, D. W., Grönvold, K., Hart, S. R., and Sachs, J. P.: Holocene loess deposition in Iceland: Evidence for millennial-scale atmosphere-ocean coupling in the North Atlantic, Geology, 33, 509–512, https://doi.org/10.1130/G21489.1, 2005.

Karnauskas, K. B., Smerdon, J. E., Seager, R., and González-Rouco, J. F.: A Pacific Centennial Oscillation Predicted by Coupled GCMs*, J. Climate, 25, 5943–5961, https://doi.org/10.1175/JCLI-D-11-00421.1, 2012.

Kobashi, T., Menviel, L., Jeltsch-Thömmes, A., Vinther, B. M., Box, J. E., Muscheler, R., Nakaegawa, T., Pfister, P. L., Döring, M., Leuenberger, M., Wanner, H., and Ohmura, A.: Volcanic influence on centennial to millennial Holocene Greenland temperature change, Sci. Rep., 7, 1441, https://doi.org/10.1038/s41598-017-01451-7, 2017.

Konecky, B. L., McKay, N. P., Falster, G. M., Stevenson, S. L., Fischer, M. J., Atwood, A. R., Thompson, D. M., Jones, M. D., Tyler, J. J., DeLong, K. L., Martrat, B., Thomas, E. K., Conroy, J. L., Dee, S. G., Jonkers, L., Churakova (Sidorova), O. V., Kern, Z., Opel, T., Porter, T. J., Sayani, H. R., and Skrzypek, G.: Globally coherent water cycle response to temperature change during the past two millennia, Nat. Geosci., 16, 997–1004, https://doi.org/10.1038/s41561-023-01291-3, 2023.

Laepple, T., Ziegler, E., Weitzel, N., Hébert, R., Ellerhoff, B., Schoch, P., Martrat, B., Bothe, O., Moreno-Chamarro, E., Chevalier, M., Herbert, A., and Rehfeld, K.: Regional but not global temperature variability underestimated by climate models at supradecadal timescales, Nat. Geosci., 16, 958–966, https://doi.org/10.1038/s41561-023-01299-9, 2023.

Larsen, D. J., Miller, G. H., Geirsdóttir, Á., and Ólafsdóttir, S.: Non-linear Holocene climate evolution in the North Atlantic: a high-resolution, multi-proxy record of glacier activity and environmental change from Hvítárvatn, central Iceland, Quaternary Sci. Rev., 39, 14–25, https://doi.org/10.1016/j.quascirev.2012.02.006, 2012.

Liu, Z., Zhu, J., Rosenthal, Y., Zhang, X., Otto-Bliesner, B. L., Timmermann, A., Smith, R. S., Lohmann, G., Zheng, W., and Timm, O. E.: The Holocene temperature conundrum, P. Natl. Acad. Sci. USA, 111, E3501–E3505, https://doi.org/10.1073/pnas.1407229111, 2014.

Lochte, A. A., Schneider, R., Kienast, M., Repschläger, J., Blanz, T., Garbe-Schönberg, D., and Andersen, N.: Surface and subsurface Labrador Shelf water mass conditions during the last 6000 years, Clim. Past, 16, 1127–1143, https://doi.org/10.5194/cp-16-1127-2020, 2020.

Ma, Z.-B., Cheng, H., Tan, M., Edwards, R. L., Li, H.-C., You, C.-F., Duan, W.-H., Wang, X., and Kelly, M. J.: Timing and structure of the Younger Dryas event in northern China, Quaternary Sci. Rev., 41, 83–93, https://doi.org/10.1016/j.quascirev.2012.03.006, 2012.

Magny, M. and Haas, J. N.: A major widespread climatic change around 5300 cal. yr BP at the time of the Alpine Iceman, J. Quaternary Sci., 19, 423–430, https://doi.org/10.1002/jqs.850, 2004.

Magny, M., Leuzinger, U., Bortenschlager, S., and Haas, J. N.: Tripartite climate reversal in Central Europe 5600–5300 years ago, Quaternary Res., 65, 3–19, 2006.

Marcott, S. A., Shakun, J. D., Clark, P. U., and Mix, A. C.: A Reconstruction of Regional and Global Temperature for the Past 11,300 Years, Science, 339, 1198–1201, https://doi.org/10.1126/science.1228026, 2013.

Marsicek, J., Shuman, B. N., Bartlein, P. J., Shafer, S. L., and Brewer, S.: Reconciling divergent trends and millennial variations in Holocene temperatures, Nature, 554, 92–96, https://doi.org/10.1038/nature25464, 2018 (data available at: https://www.ncdc.noaa.gov/paleo-search/study/22992, last access: 7 October 2023).

Marsicek, J. P., Shuman, B., Brewer, S., Foster, D. R., and Oswald, W. W.: Moisture and temperature changes associated with the mid-Holocene Tsuga decline in the northeastern United States, Quaternary Sci. Rev., 80, 333–342, https://doi.org/10.1016/j.quascirev.2013.09.001, 2013.

Martínez-Sosa, P., Tierney, J. E., Stefanescu, I. C., Dearing Crampton-Flood, E., Shuman, B. N., and Routson, C.: A global Bayesian temperature calibration for lacustrine brGDGTs, Geochim. Cosmochim. Ac., 305, 87–105, https://doi.org/10.1016/j.gca.2021.04.038, 2021.

Mayewski, P. A., Rohling, E., Stager, C., Karlen, K., Maasch, K., Meeker, L. D., Meyerson, E., Gasse, F., van Kreveld, S., Holmgren, K., Lee-Thorp, J., Rosqvist, G., Rack, F., Staubwasser, M., and Shneider, R.: Holocene climate variability, Quaternary Res., 62, 243, https://doi.org/10.1016/j.yqres.2004.07.001, 2004.

Muschitiello, F., Zhang, Q., Sundqvist, H. S., Davies, F. J., and Renssen, H.: Arctic climate response to the termination of the African Humid Period, Quaternary Sci. Rev., 125, 91–97, https://doi.org/10.1016/j.quascirev.2015.08.012, 2015.

Nelson, D. M. and Hu, F. S.: Patterns and drivers of Holocene vegetational change near the prairie-forest ecotone in Minnesota: revisiting McAndrews' transect, New Phytol., 179, 449–459, 2008.

Newby, P., Shuman, B., Donnelly, J. P., Karnauskas, K. B., and Marsicek, J. P.: Centennial-to-Millennial Hydrologic Trends and Variability along the North Atlantic Coast, U.S.A., during the Holocene, Geophys. Res. Lett., 41, 4300–4307, https://doi.org/10.1002/2014GL060183, 2014 (data available at: https://www.ncdc.noaa.gov/paleo-search/study/23074, last access: 7 October 2023).

Newby, P. E., Shuman, B. N., Donnelly, J. P., and MacDonald, D.: Repeated century-scale droughts over the past 13,000 yrs near

the Hudson River watershed, USA, Quaternary Res., 75, 523–530, 2011.

NOAA NCEI: ETOPO 2022 15 Arc-Second Global Relief Model, NOAA National Centers for Environmental Information, https://doi.org/10.25921/fd45-gt74, 2022.

Olsen, J., Anderson, N. J., and Knudsen, M. F.: Variability of the North Atlantic Oscillation over the past 5,200 years, Nat. Geosci., 5, 808–812, https://doi.org/10.1038/ngeo1589, 2012.

Oppo, D. W., McManus, J. F., and Cullen, J. L.: Palaeooceanography: Deepwater variability in the Holocene epoch, Nature, 422, 277–277, 2003.

Orme, L. C., Miettinen, A., Seidenkrantz, M.-S., Tuominen, K., Pearce, C., Divine, D. V., Oksman, M., and Kuijpers, A.: Mid to late-Holocene sea-surface temperature variability off north-eastern Newfoundland and its linkage to the North Atlantic Oscillation, The Holocene, 31, 3–15, https://doi.org/10.1177/0959683620961488, 2021.

Osman, M. B., Tierney, J. E., Zhu, J., Tardif, R., Hakim, G. J., King, J., and Poulsen, C. J.: Globally resolved surface temperatures since the Last Glacial Maximum, Nature, 599, 239–244, https://doi.org/10.1038/s41586-021-03984-4, 2021.

PAGES 2k Consortium: Continental-scale temperature variability during the past two millennia, Nat. Geosci., 6, 339–346, https://doi.org/10.1038/NGEO1797, 2013.

Parnell, A. C., Haslett, J., Allen, J. R. M., Buck, C. E., and Huntley, B.: A flexible approach to assessing synchroneity of past events using Bayesian reconstructions of sedimentation history, Quaternary Sci. Rev., 27, 1872–1885, https://doi.org/10.1016/j.quascirev.2008.07.009, 2008.

Pausata, F. S. R., Messori, G., and Zhang, Q.: Impacts of dust reduction on the northward expansion of the African monsoon during the Green Sahara period, Earth Planet. Sc. Lett., 434, 298–307, https://doi.org/10.1016/j.epsl.2015.11.049, 2016.

Percival, D. B. and Walden, A. T.: Spectral Analysis for Physical Applications, Cambridge University Press, 616 pp., ISBN 0-521-43541-2, 1993.

Puleo, P. J. K., Axford, Y., McFarlin, J. M., Curry, B. B., Barklage, M., and Osburn, M. R.: Late glacial and Holocene paleoenvironments in the midcontinent United States, inferred from Geneva Lake leaf wax, ostracode valve, and bulk sediment chemistry, Quaternary Sci. Rev., 241, 106384, https://doi.org/10.1016/j.quascirev.2020.106384, 2020.

R Core Development Team: R: A language and environment for statistical computing, R Foundation for Statistical Computing, Vienna, Austria, https://www.r-project.org/ (last access: 12 February 2024), 2020.

Rach, O., Brauer, A., Wilkes, H., and Sachse, D.: Delayed hydrological response to Greenland cooling at the onset of the Younger Dryas in western Europe, Nat. Geosci., 7, 109–112, https://doi.org/10.1038/ngeo2053, 2014.

Renssen, H., Goosse, H., and Muscheler, R.: Coupled climate model simulation of Holocene cooling events: oceanic feedback amplifies solar forcing, Clim. Past, 2, 79–90, https://doi.org/10.5194/cp-2-79-2006, 2006.

Reschke, M., Kunz, T., and Laepple, T.: Comparing methods for analysing time scale dependent correlations in irregularly sampled time series data, Comput. Geosci., 123, 65–72, https://doi.org/10.1016/j.cageo.2018.11.009, 2019.

Russell, J. M., Hopmans, E. C., Loomis, S. E., Liang, J., and Sinninghe Damsté, J. S.: Distributions of 5- and 6-methyl branched glycerol dialkyl glycerol tetraethers (brGDGTs) in East African lake sediment: Effects of temperature, pH, and new lacustrine paleotemperature calibrations, Org. Geochem., 117, 56–69, https://doi.org/10.1016/j.orggeochem.2017.12.003, 2018.

Sachs, J. P.: Cooling of Northwest Atlantic slope waters during the Holocene, Geophys. Res. Lett., 34, L03609, https://doi.org/10.1029/2006gl028495, 2007 (data available at: https://www.ncdc.noaa.gov/paleo-search/study/6409, last access: 7 October 2023).

Saltzman, B.: Stochastically-driven climatic fluctuations in the sea-ice, ocean temperature, CO_2 feedback system, Tellus, 34, 97–112, https://doi.org/10.1111/j.2153-3490.1982.tb01797.x, 1982.

Schmidt, M. W., Weinlein, W. A., Marcantonio, F., and Lynch-Stieglitz, J.: Solar forcing of Florida Straits surface salinity during the early Holocene, Paleoceanography, 27, PA3204, https://doi.org/10.1029/2012PA002284, 2012.

Shuman, B. N. and Burrell, S. A.: Centennial to millennial hydroclimatic fluctuations in the humid northeast United States during the Holocene, Quaternary Res., 88, 514–524, https://doi.org/10.1017/qua.2017.62, 2017.

Shuman, B. N. and Marsicek, J. P.: The Structure of Holocene Climate Change in Mid-Latitude North America, Quaternary Sci. Rev., 141, 38–51, https://doi.org/10.1016/j.quascirev.2016.03.009, 2016 (data available at: https://www.ncdc.noaa.gov/paleo-search/study/31097, last access: 7 October 2023).

Shuman, B. N., Carter, G. E., Hougardy, D. D., Powers, K., and Shinker, J. J.: A north–south moisture dipole at multi century scales in the Central and Southern Rocky Mountains during the late Holocene, Rocky Mt. Geol., 49, 17–33, 2014.

Shuman, B. N., Marsicek, J., Oswald, W. W., and Foster, D. R.: Predictable hydrological and ecological responses to Holocene North Atlantic variability, P. Natl. Acad. Sci. USA, 116, 5985–5990, https://doi.org/10.1073/pnas.1814307116, 2019.

Shuman, B. N., Stefanescu, I. C., Grigg, L., Foster, D. R., and Oswald, W. W.: A Millennial-Scale Oscillation in Latitudinal Temperature Gradients along the Western North Atlantic during the Mid-Holocene, Geophys. Res. Lett., 50, e2022GL102556, https://doi.org/10.1029/2022GL102556, 2023.

Slutzky, E.: The Summation of Random Causes as the Source of Cyclic Processes, Econometrica, 5, 105–146, https://doi.org/10.2307/1907241, 1937.

Smith, A. J., Donovan, J. J., Ito, E., Engstrom, D. R., and Panek, V. A.: Climate-driven hydrologic transients in lake sediment records: multoproxy record of mid-Holocene drought, Quaternary Sci. Rev., 21, 625–646, https://doi.org/10.1016/S0277-3791(01)00041-5, 2002.

Steinman, B. A., Rosenmeier, M. F., and Abbott, M. B.: The isotopic and hydrologic response of small, closed-basin lakes to climate forcing from predictive models: Simulations of stochastic and mean state precipitation variations, Limnol. Oceanogr., 55, 2246–2261, https://doi.org/10.4319/lo.2010.55.6.2246, 2010.

Telford, R. J. and Birks, H. J. B.: A novel method for assessing the statistical significance of quantitative reconstructions inferred from biotic assemblages, Quaternary Sci. Rev., 30, 1272–1278, https://doi.org/10.1016/j.quascirev.2011.03.002, 2011.

Thompson, L. G., Mosley-Thompson, E., Davis, M. E., Henderson, K. A., Brecher, H. H., Zagorodnov, V. S., Mashiotta, T. A., Lin, P.-N., Mikhalenko, V. N., Hardy, D. R., and Beer, J.: Kilimanjaro Ice Core Records: Evidence of Holocene Climate Change in Tropical Africa, Science, 298, 589–593, https://doi.org/10.1126/science.1073198, 2002.

Thornalley, D. J. R., Elderfield, H., and McCave, I. N.: Holocene oscillations in temperature and salinity of the surface subpolar North Atlantic, Nature, 457, 711–714, 2009.

Wan, L., Liu, Z., Liu, J., Sun, W., and Liu, B.: Holocene temperature response to external forcing: assessing the linear response and its spatial and temporal dependence, Clim. Past, 15, 1411–1425, https://doi.org/10.5194/cp-15-1411-2019, 2019.

Wanner, H., Beer, J., Bütikofer, J., Crowley, T. J., Cubasch, U., Flückiger, J., Goosse, H., Grosjean, M., Joos, F., Kaplan, J. O., Küttel, M., Müller, S. A., Prentice, I. C., Solomina, O., Stocker, T. F., Tarasov, P., Wagner, M., and Widmann, M.: Mid- to Late Holocene climate change: an overview, Quaternary Sci. Rev., 27, 1791–1828, 2008.

Willard, D. A., Bernhardt, C. E., Korejwo, D. A., and Meyers, S. R.: Impact of millennial-scale Holocene climate variability on eastern North American terrestrial ecosystems: pollen-based climatic reconstruction, Global Planet. Change, 47, 17–35, https://doi.org/10.1016/j.gloplacha.2004.11.017, 2005.

Williams, J. W. and Shuman, B.: Obtaining accurate and precise environmental reconstructions from the modern analog technique and North American surface pollen dataset, Quaternary Sci. Rev., 27, 669–687, 2008.

Wills, R. C. J., Armour, K. C., Battisti, D. S., and Hartmann, D. L.: Ocean–Atmosphere Dynamical Coupling Fundamental to the Atlantic Multidecadal Oscillation, J. Climate, 32, 251–272, https://doi.org/10.1175/JCLI-D-18-0269.1, 2019.